Creation of Orbital Angular Momentum States with Chiral Polaritonic Lenses

Robert Dall,[1,2] Michael D. Fraser,[3] Anton S. Desyatnikov,[1] Guangyao Li,[1] Sebastian Brodbeck,[4] Martin Kamp,[4] Christian Schneider,[4] Sven Höfling,[4,5] and Elena A. Ostrovskaya[1]

[1]*Nonlinear Physics Centre, The Australian National University, Canberra ACT 0200, Australia*

[2]*AMPL, Research School of Physics and Engineering, The Australian National University, Canberra ACT 0200, Australia*

[3]*Quantum Functional System Research Group, RIKEN Center for Emergent Matter Science, 2-1 Hirosawa, Wako-shi, Saitama 351-0198, Japan*

[4]*Technische Physik and Wilhelm-Conrad-Röntgen Research Center for Complex Material Systems, Universität Würzburg, D-97074 Würzburg, Germany*

[5]*School of Physics and Astronomy, University of St Andrews, St Andrews, Fife, KY16 9SS, United Kingdom*

(Received 30 June 2014; published 12 November 2014)

Controlled transfer of orbital angular momentum to an exciton-polariton Bose-Einstein condensate spontaneously created under incoherent, off resonant excitation conditions is a long-standing challenge in the field of microcavity polaritonics. We demonstrate, experimentally and theoretically, a simple and efficient approach to the generation of nontrivial orbital angular momentum states by using optically induced potentials—chiral polaritonic lenses. These lenses are produced by a structured optical pump with a spatial distribution of intensity that breaks the chiral symmetry of the system.

DOI: 10.1103/PhysRevLett.113.200404 PACS numbers: 03.75.Lm, 67.85.De, 71.36.+c

Introduction.—Recent advances in optical excitation and manipulation of exciton-polaritons in semiconductor microcavities lead to the creation and trapping of a polariton Bose-Einstein condensate [1] in optically induced potentials [2–6]. These potentials are created by incoherent optical sources of exciton-polaritons due to self-trapping mechanisms that are inherent in this open-dissipative system [7–9] and are similar to those at play in optical systems with gain and loss [10–12]. The advantage of the "soft", optically-induced potentials over those "hard wired" in the microcavity, e.g., by etching process [13], is the ability to reconfigure their spatial and energy landscape by structuring the optical pump.

A long-standing and so far unsolved problem in exciton-polariton physics is the inability to transfer orbital angular momentum directly from the optical pump to the spontaneously condensed exciton-polaritons. The effective potentials created by an optical pump via an uncondensed reservoir of high-energy near-excitonic polaritons depend only on the pump intensity, and all of the phase information is "scrambled" in the process of energy relaxation. This is in stark contrast to a condensate of ultracold atoms that admits direct imprinting of quantum states of photons [14] and to coherently driven polaritons in the resonant excitation schemes [15–17]. The solution of this problem holds the key to controlled creation of quantized orbital angular momentum states and persistent currents, which could be employed in the polariton analogue of superconducting quantum interference device (SQUID) sensors [18–20] and information encoding devices [21], as well as in the fundamental studies of vortices [22] and polariton Bose-Einstein condensates under rotation. So far, vortices in an incoherently excited exciton-polariton condensate have only been generated spontaneously and, in the absence of total angular momentum in the system, only in the form of vortex-antivortex pairs [23–27] or degenerate spin vortices [28,29].

In this Letter, we show that chiral polaritonic lenses—potentials with broken chiral symmetries—enable reliable creation of nontrivial orbital angular momentum states in spontaneously formed exciton-polariton Bose-Einstein condensates. Such lenses are formed by an off resonant optical pump with a chiral distribution of intensity [Fig. 1(a)] structured with a pinhole optical mask. Chirality of the lens can be accidental due to small beam shifts relative to the mask [Fig. 1(b)] or engineered by varying the size or position of pinholes [Figs. 1(d) and 1(e)]. In particular, we demonstrate efficient creation of a single charge vortex by a spiral polaritonic lens in Fig. 1(e). This method represents a new paradigm in the control of orbital angular momentum states of light and matter, with the schemes previously demonstrated in optics [30,31], plasmonics [32], ultracold atom physics [14,33], and polaritonics [16,17] relying on chiral distributions of phase created by coherent, resonant sources and processes.

Experiment.—In an experiment, we work with an GaAs/AlGaAs microcavity sandwiched between distributed Bragg reflector mirrors to achieve high confinement of a photon mode [34]. In the regime of strong coupling between the photons and excitons confined in 2D quantum wells imbedded in the microcavity, exciton-polaritons form and can be driven to a Bose-Einstein condensation. The condensation occurs spontaneously above a threshold power of the pumping laser.

The cw optical pump, with the excitation energy far above the exciton or polariton resonance, is a broad

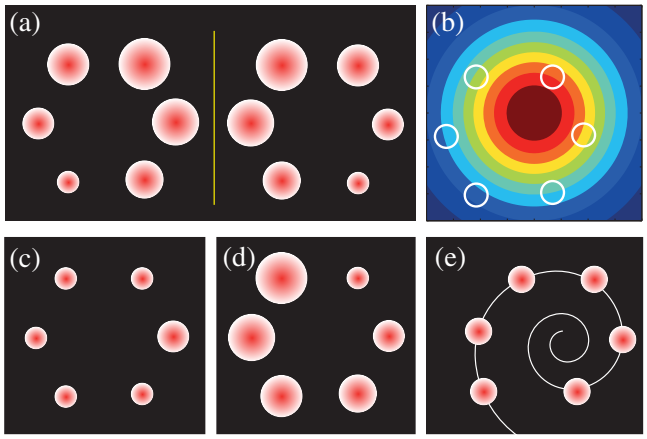

FIG. 1 (color online). Schematics of the optical pump structured via a six-pinhole metal mask. (a) Spatial distribution of the intensity shown together with its mirror image to demonstrate chirality; the pump structure cannot be superimposed with its mirror image by simple rotation. Chirality appears due to an accidental misalignment as shown in (b); (b) Gaussian pump beam shifted relative to the mask center, resulting in the spatial intensity distribution shown in (a); (c)–(e) Engineered intensity distributions of the (c) nonchiral and (d), (e) chiral polaritonic lenses tested in experiment. In (a), the intensity of the pump spots is represented by their size, and the degree of asymmetry in (a), (c)–(e) is exaggerated for clarity.

Gaussian beam spatially modulated in the near field by a metal mask patterned with an arbitrary configuration of holes, and subsequently, reimaged onto the microcavity sample surface at normal incidence. It allows us to create an azimuthal distribution of pump spots responsible for trapping of the condensate in the center of the effective trap produced by the polaritonic lens, similarly to the experiments involving spatial light modulators [5,6]. The mask enables us to create structured potentials of arbitrary shape with stability limited only by stability of the laser. For this work, in particular, we use a six-spot azimuthal intensity distribution.

As the mask is reimaged on the surface of the sample, the size of the potential is determined by the depth of focus. In the current experiment, pump spots of 3 μm at a 7 μm spacing, with the typical size of the resulting condensate $\sim$5 μm. The imaging system consists of a free-space microscope with a high numerical aperture objective, which collects the photoluminescence from the sample, and allows us to infer both the spatial and momentum distribution of condensed polaritons from emitted photons. The pump is linearly polarized and the resulting photoluminescence appears to be largely unpolarized. A Michelson interferometer is used to analyze the phase structure of the signal [34].

Control of the polariton flow with a structured optical pump relies on two experimentally verified processes. First, several pump spots in close proximity of each other create phase-locked condensates [3,4]. Secondly, nonlinear interaction between the polaritons and a reservoir creates an effective trapping potential with the depth proportional to the strength of the pump [5,6]. The spatial distribution of the condensate density is affected by the pump intensity. This could be understood from a simple linear interference picture. In the far field of each individual pump spot, in the plane of the quantum well, the polariton matter wave can be approximated by a wave packet with a radially symmetric phase front and exponentially decaying envelope [8]: $\psi_c \sim \exp(-\Gamma r)\exp(i\mathbf{k}_p\mathbf{r})$. As the intensity of the pump increases, so does the chemical potential (energy of the steady state) of the condensate, μ, [8,35], and both the wavelength of the polariton matter wave, $\lambda_p \sim 1/k_p$, and the width of the condensate decrease as $\{\lambda_p, \Gamma\} \sim \mu^{-1/2}$ [8]. For the perfectly symmetric ringlike configuration of six identical pump spots, the superposition of long-wavelength condensate "tails" would tend to localize the density in the excitation regions for a weaker pump intensity (larger λ_p and Γ) [Fig. 2(a)]. A higher pump intensity (smaller λ_p and Γ) would produce a bright spot in the center [Fig. 2(c)]. In the latter regime, the structured pump works as a lens, focusing the condensate into the center. These spatial patterns will be amplified due to the stimulated scattering of polaritons into the regions of high density and therefore, lead to different spatial structures of the condensate at different pump powers, as seen in the experiment [Figs. 2(b) and 2(d)].

The condensate formed in the center of the polaritonic lens just above the condensation threshold is almost perfectly radially symmetric [Fig. 3(a)], and can be thought of as a ground state of a radially symmetric 2D potential well effectively created by the pump through induced spatial distribution of the reservoir density [5,6]. In the polar coordinates, the eigenstates of this potential can be written as $\psi_{n,m} = \Phi_n(r)\exp(im\theta)$. The first excited energy state produced by a stronger pump is a dipole mode superposition [Fig. 3(b)] of two $n = 1$ states with the nonzero orbital angular momentum, i.e., quantized vortices with topological charge $m = +1$ and $m = -1$. The second excited state is a quadrupole mode superposition (not shown) of $n = 2$ vortex states with the topological charge $m = +2$ and $m = -2$ and a state with $m = 0$ containing a radial node. The total topological charge and orbital

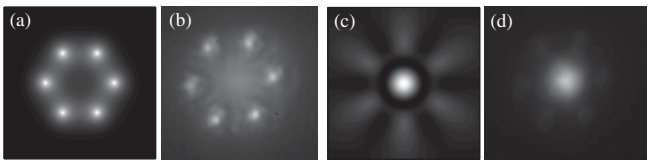

FIG. 2. Schematic illustration of the linear interference of six phase coherent polariton condensates (a) at low pump intensity, where the fringes are absent due to the long wavelength; (c) at high pump intensity (see text). Panels (b), (d) show the respective experimental real-space images (b) at and (d) above condensation threshold corresponding to Figs. S3(b) and S3(c).

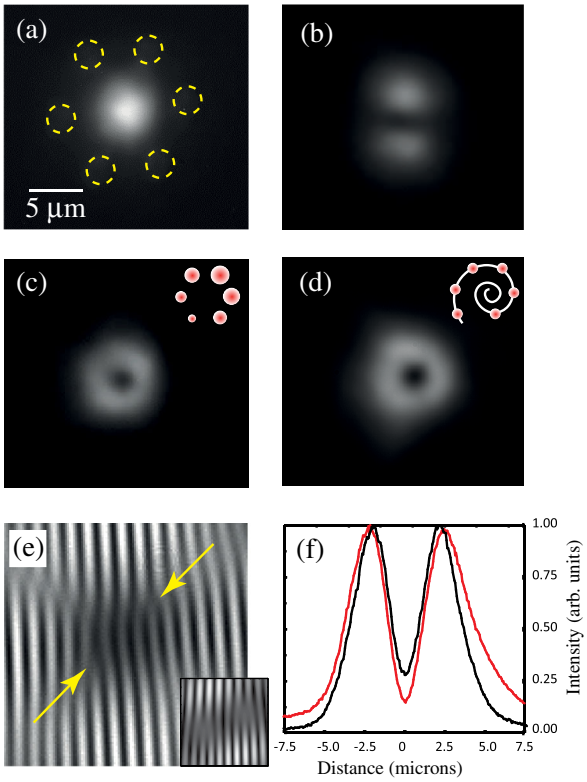

FIG. 3 (color online). Experimental real space image of cavity emission intensity showing (a) ground state ($|m| = 0$), (b) dipole mode ($|m| = 0$), and (c), (d) charge one vortices ($|m| = 1$) created by the polaritonic lenses in Figs. 1(a) and 1(e). Circles in (a) mark positions of pump spots; (e) Experimental and (inset) theoretical interference pattern of retroreflected far-field photoluminescence from the charge one vortex in (d). Arrows mark locations of "forks" indicating presence of a single isolated vortex in the center of the condensate. (d) Intensity profiles of the vortices in (c), (d) obtained with accidentally (black line) and deliberately engineered (red line) chiral lens at the pump intensities marked by dashed lines in Figs. 4(a) and 4(b). Images in (a)–(d) are plotted on the same scale, and the interferometric image (e) is magnified for clarity.

angular momentum of the superposition states is zero. To select a mode with nonzero topological charge, one needs to break the chiral symmetry of the lens.

Even a slight misalignment of the Gaussian pump beam with the center of the metal mask used to reimage sophisticated spatial distribution of intensity onto the surface of the sample can create symmetry breaking in the polaritonic lens [Figs. 1(c) and 1(d)]. As shown in Fig. 1, the resulting structures can be nonchiral (c) or chiral (a),(d). At a low pump power, the accidental chirality is weak, and the resulting higher-order state observed in the experiment still resembles a dipole mode [Fig. 3(b)]. However, as the pump intensity grows, the mode selection strongly favors a single charge one vortex, $m = \pm 1$, clearly visible both in real space images [Fig. 3(c)] and interferometric images [Fig. 3(e)] of the photoluminescence signal. Thus, accidental chirality forces the polariton condensate into a nonzero orbital angular momentum state.

The mode selection of a vortex state is much more efficient in polaritonic lenses with an engineered chirality. In the experiment, we tested both the circular masks with different hole sizes [as shown in Fig. 1(d)] and the spiral masks with identical holes [Fig. 1(e)]. The efficiency of the mode selection is quantified via the energy resolved measurement of the mode population vs pump power. As seen in Fig. 4(b), the engineered chiral structure strongly suppresses formation of the ground state condensate with a zero orbital angular momentum [34]. The ground state mode clearly visible in Fig. 4(a) at lower powers, e.g., at ~10 mW, is very weakly populated in Fig. 4(b). The vortex $m = \pm 1$ state produced by the engineered chiral lens has a stronger admixture of the $m = \pm 2$ state, which results in a much greater contrast, defined through the minimum and maximum intensity of the photoluminescence as $I_c = (I_{\max} - I_{\min})/I_{\max}$. The admixture of the ground state causes the contrast to deviate from one (for a perfect zero intensity in the vortex core). For the vortex produced with the engineered chiral structure in our experiments [Fig. 3 (d)], the best contrast is $I_c \approx 0.82$ [at $P = 12.5$ mW, dashed line in Fig. 4(b)], whereas the best contrast achieved for the accidental chirality is $I_c \approx 0.76$ [at $P = 22.5$ mW, dashed line in Fig. 4(a)]. We note that the efficient mode selection by the incoherent polaritonic lens represents more than a twofold improvement on the contrast $I_c \approx 0.38$ reported in the coherent vortex excitation experiments via the resonant OPO scheme [16].

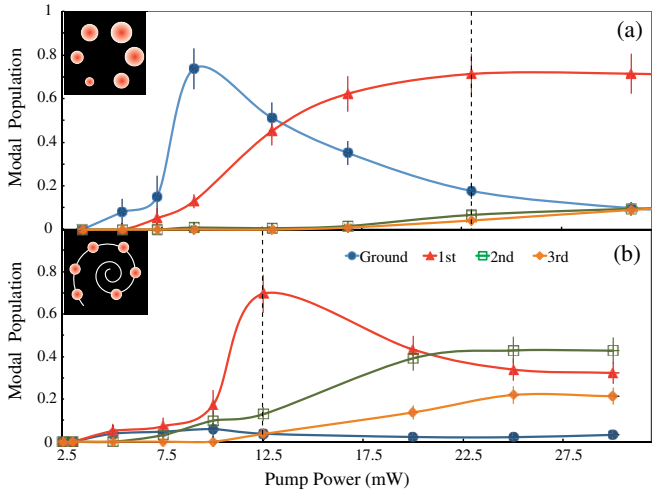

FIG. 4 (color online). Experimental measurement of relative populations of the ground ($n = 0$), first ($n = 1$), and higher-order ($n = 2, 3$) energy states of the effective trap induced by the polaritonic lens with an (a) accidental and an (b) engineered chirality. The populations are normalized by the total density of condensed and uncondensed ("thermal") polaritons [36]. The condensation threshold in both cases is $P_{\text{th}} \approx 5$ mW. Solid lines are a guide to the eye. Dashed lines mark vortex states ($|m| = 1$) shown in Figs. 3(c) and 3(d).

Modeling.—We consider a spontaneously formed exciton-polariton condensate under the continuous wave far off resonant optical excitation injecting free carriers into the system high above the lower polariton energy. The model consists of a mean-field equation for the polariton condensate wave function and a rate equation for the inhomogeneous density of the reservoir [37]:

$$i\hbar\frac{\partial\Psi}{\partial t} = \left[-\frac{\hbar^2}{2m}\nabla_\perp^2 + V(\vec{r},t) + i\frac{\hbar}{2}(Rn_R - \gamma_c)\right]\Psi,$$
$$\frac{\partial n_R}{\partial t} = -(\gamma_R + R|\Psi|^2)n_R(\vec{r},t) + P(\vec{r}), \quad (1)$$

where $V(\vec{r},t) = g_c|\Psi|^2 + g_R n_R(\vec{r},t)$. Here, Ψ is the condensate wave function, n_R is the reservoir density, and $P(\vec{r})$ is the spatially modulated optical pumping rate. The critical parameters defining the condensate dynamics are the loss rates of the polaritons γ_c and reservoir polaritons γ_R, the stimulated scattering rate R, and the strengths of polariton-polariton, g_c, and polariton-reservoir, g_R, interactions. In what follows, we use the dimensionless form of the model obtained by using the scaling units of time, energy, and length: $T = 1/\gamma_c$, $E = \hbar\gamma_c$, $L = [\hbar/(m_{LP}\gamma_c)]^{1/2}$, where m_{LP} is the lower-polariton effective mass [38].

We model both chiral and nonchiral polaritonic lenses with very small asymmetries, so that the spot-to-spot variation of intensity similar to that shown in Fig. 1(a) is $1\% \leq \delta P \leq 5\%$. First, we model the weakly unbalanced nonchiral lens shown in Fig. 1(c). These are produced, e.g., by beam shifts along a symmetry axis of the mask. For the pump intensity at threshold and no symmetry breaking ($\delta P = 0$), formation of ground state condensate with peak density in the geometrical center was seen in numerical calculations and in our experiments, and was also observed in recent experiments [5] for similar polaritonic lenses of small radii. In numerical simulations, the threshold for condensation is roughly determined by the ratio $P_{\text{th}} = \gamma_R\gamma_c/R$ [37].

Even the weak symmetry breaking results in a drastically different polariton density distribution. Above the threshold, the condensate favors formation of a steady state with the dipole-mode structure [Fig. 5(a)]. In simulations, the two lobes of the dipole are separated by a phase fold binding a stable vortex-antivortex pair. Such pairs may form spontaneously due to nonlinearity-induced instabilities [39] and are destroyed as they move to the periphery of the condensate, unless a special density profile is engineered to hold them in place [27]. The remarkable feature here is the survival of a single stable vortex-antivortex pair and the resulting formation of the stationary dipole mode. We stress that, since the polaritonic lens is nonchiral, the system does not distinguish between left- and right-hand circulation of polariton flows. Thus, the symmetry breaking of this kind cannot lead to generation of a single isolated vortex in the system.

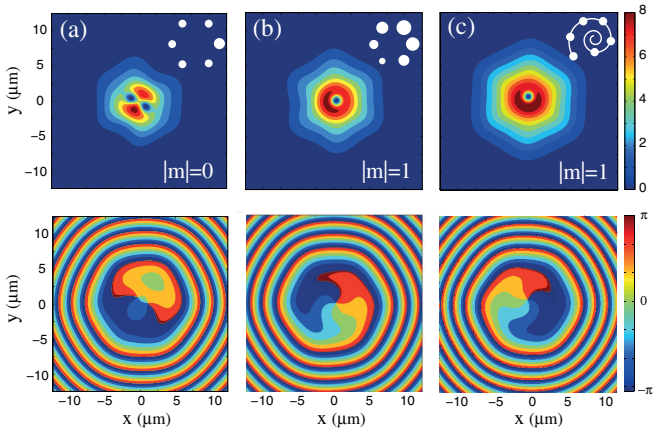

FIG. 5 (color online). Modeled steady state real-space density (top row) and phase (bottom row) created with (a) the nonchiral hexagonal polaritonic lens shown in Fig. 1(c) for the unbalanced pump with $P/P_{\text{th}} = 1.17$; (b) polaritonic lens with accidental chirality with $P/P_{\text{th}} = 1.2$; (c) the engineered chiral lens. Insets show schematic configuration of the polaritonic lenses, and $|m|$ indicates total topological charge of the resulting structure.

Next, we model the lenses with an accidental [Figs. 1(a) and 1(b)] or an engineered [Figs. 1(d) and 1(e)] chirality. The drastic consequence of the introduced handedness of the system is the formation and stabilization of steady states containing single vortices [Figs. 5(b) and 5(c)]. We stress that the vortices appear strictly due to the symmetry breaking in the chiral polaritonic lens and, in numerical modeling, no vorticity was "seeded" into the system. In principle, vortices of various topological charge corresponding to the different degree of asymmetry in the system can be generated. Preliminary experimental and theoretical results on formation of the $|m| = 2$ state are presented in the Supplemental Material (section IV) [34]. The detailed study of this process will be reported elsewhere.

We also note that the model [Eq. (1)] does capture the experimentally observed resemblance of the collective polariton modes to eigenstates of a linear potential well created in the middle of a polaritonic lens. Indeed, according to the model, the effective linear potential created for polaritons $V_{\text{lin}} \sim (g_R\gamma_c/R)\bar{P}(\mathbf{r})$, where $\bar{P} = P/P_{\text{th}}$, takes the form of the strongly repulsive (antitrapping) barrier localized around the periphery of the polaritonic lens, thus creating a trap in the middle. The self-induced nonlinear contribution to the potential due to polariton interactions is, to the leading order, $V_{\text{nl}} \sim g_c[1 - \bar{P}(\mathbf{r})(g_R\gamma_c)/(g_c\gamma_R)]|\Psi|^2$, and therefore, acts to enhance the trapping potential for the chosen parameters, which agrees well with previous studies [5,6] and our experimental observations.

Conclusions.—We have demonstrated an operation of chiral polaritonic lenses for the reliable creation and trapping of incoherently excited polariton condensates with nonzero orbital angular momentum, containing single

vortices. The role of the broken symmetry in such lenses is two fold: first, in the presence of strong polariton interactions, it triggers the development of nonlinear instabilities leading to formation of phase vortices and antivortices, and secondly, the distinct handedness of the system leads to selection of steady states with isolated single vortices and overall nonzero orbital angular momentum.

The deliberately created isolated vortex states are robust, reproducible, and persist for hours, i.e., for as long as the exciton-polariton condensate is maintained by the cw optical pump. Our findings open the way to construction of all-optical elements for shaping and directing of polariton flows with a well-defined orbital angular momentum, which could be captured by potentials "hard wired" in a microcavity, and used for study of vortices and persistent currents.

It is tempting to draw parallels between the optical manipulation of exciton polaritons in the plane of the quantum well and shaping of radiation by means of surface plasmon-polariton lenses [32]. However, as stressed in the introduction, shaping of the optical wave front in the coherently illuminated nanostructures relies on precise spiral phase distribution introduced by the asymmetrically placed coherent sources. In contrast, formation of vortex states in an incoherently excited exciton-polariton condensate is a result of the mode selection in an effective potential induced by a spiral intensity distribution, and therefore, is much less sensitive to the precise geometry of the structured pump. Although exciton polaritons allow us to manipulate light on the microscale rather than a nanoscale, the ultrafast velocities and strong nonlinearities inherent to exciton polaritons and unavailable in plasmonics could potentially enable novel optoelectronic devices.

This work was supported by the Australian Research Council (ARC), the State of Bavaria, and Japan Society for the Promotion of Science (JSPS) through its "Funding Program for World-Leading Innovative R&D on Science and Technology (FIRST Program). We are indebted to K. Y. Bliokh for careful reading of the manuscript and in-depth comments. Discussions with I. V. Shadrivov and Yu. S. Kivshar are gratefully acknowledged.

[1] J. Kasprzak, M. Richard, S. Kundermann, A. Baas, P. Jeambrun, J. M. J. Keeling, F. M. Marchetti, M. H. Szymańska, R. André, J. L. Staehli, V. Savona, P. B. Littlewood, B. Deveaud, and Le Si Dang, Nature (London) **443**, 409 (2006); H. Deng, H. Haug, and Y. Yamamoto, Rev. Mod. Phys. **82**, 1489 (2010); I. Carusotto and C. Ciuti, Rev. Mod. Phys. **85**, 299 (2013).

[2] F. Manni, K. G. Lagoudakis, T. C. H. Liew, R. André, and B. Deveaud-Plédran, Phys. Rev. Lett. **107**, 106401 (2011).

[3] G. Tosi, G. Christmann, N. G. Berloff, P. Tsotsis, T. Gao, Z. Hatzopoulos, P. G. Savvidis, and J. J. Baumberg, Nat. Phys. **8**, 190 (2012).

[4] G. Tosi, G. Christmann, N. G. Berloff, P. Tsotsis, T. Gao, Z. Hatzopoulos, P. G. Savvidis, and J. J. Baumberg, Nat. Commun. **3**, 1243 (2012).

[5] P. Cristofolini, A. Dreismann, G. Christmann, G. Franchetti, N. G. Berloff, P. Tsotsis, Z. Hatzopoulos, P. G. Savvidis, and J. J. Baumberg, Phys. Rev. Lett. **110**, 186403 (2013).

[6] A. Askitopoulos, H. Ohadi, A. V. Kavokin, Z. Hatzopoulos, P. G. Savvidis, and P. G. Lagoudakis, Phys. Rev. B **88**, 041308(R) (2013).

[7] G. Roumpos, W. H. Nitsche, S. Höfling, A. Forchel, and Y. Yamamoto, Phys. Rev. Lett. **104**, 126403 (2010).

[8] E. A. Ostrovskaya, J. Abdullaev, A. S. Desyatnikov, M. D. Fraser, and Yu. S. Kivshar, Phys. Rev. A **86**, 013636 (2012).

[9] L. Ge, A. Nersisyan, B. Oztop, and H. E. Türeci, arXiv: 1311.4847 (2013).

[10] N. N. Rozanov, S. V. Fedorov, and A. N. Shatsev, JETP **98**, 427 (2004).

[11] A. Ankiewicz, N. Devine, N. Akhmediev, and J. M. Soto-Crespo, Phys. Rev. A **77**, 033840 (2008).

[12] D. A. Zezyulin, Y. V. Kartashov, and V. V. Konotop, Opt. Lett. **36**, 1200 (2011).

[13] O. El Daïf, A. Baas, T. Guillet, J.-P. Brantut, R. Idrissi Kaitouni, J. L. Staehli, F. Morier-Genoud, and B. Deveaud, Appl. Phys. Lett. **88**, 061105 (2006).

[14] M. F. Andersen, C. Ryu, P. Cladé, V. Natarajan, A. Vaziri, K. Helmerson, and W. D. Phillips, Phys. Rev. Lett. **97**, 170406 (2006).

[15] D. Sanvitto, F. M. Marchetti, M. H. Szymańska, G. Tosi, M. Baudisch, F. P. Laussy, D. N. Krizhanovskii, M. S. Skolnick, L. Marrucci, A. Lemaître, J. Bloch, C. Tejedor, and L. Viña, Nat. Phys. **6**, 527 (2010).

[16] D. N. Krizhanovskii, D. M. Whittaker, R. A. Bradley, K. Guda, D. Sarkar, D. Sanvitto, L.Vina, E. Cerda, P. Santos, K. Biermann, R. Hey, and M. S. Skolnick, Phys. Rev. Lett. **104**, 126402 (2010).

[17] G. Tosi, D. Sanvitto, M. Baudisch, E. Karimi, B. Piccirillo, L. Marrucci, A. Lemaitre, J. Bloch, and L. Vina, J. Appl. Phys. **109**, 102406 (2011).

[18] A. Ramanathan, K. C. Wright, S. R. Muniz, M. Zelan, W. T. Hill, C. J. Lobb, K. Helmerson, W. D. Phillips, and G. K. Campbell, Phys. Rev. Lett. **106**, 130401 (2011).

[19] C. Ryu, P. W. Blackburn, A. A. Blinova, and M. G. Boshier, Phys. Rev. Lett. **111**, 205301 (2013).

[20] G. Franchetti, N. G. Berloff, and J. J. Baumberg, arXiv: 1210.1187.

[21] K. T. Kapale and J. P. Dowling, Phys. Rev. Lett. **95**, 173601 (2005).

[22] A. L. Fetter and A. A. Svidzinsky, J. Phys. Condens. Matter **13**, R135 (2001).

[23] K. G. Lagoudakis, M. Wouters, M. Richard, A. Baas, I. Carusotto, R. Andre, L. Si Dang, and B. Deveaud-Plédran, Nat. Phys. **4**, 706 (2008).

[24] G. Roumpos, M. D. Fraser, A. Löffler, S. Höfling, A. Forchel, and Y. Yamamoto, Nat. Phys. **7**, 129 (2011).

[25] G. Nardin, G. Grosso, Y. Léger, B. Piętka, F. Morier-Genoud, and B. Deveaud-Plédran, Nat. Phys. **7**, 635 (2011).

[26] D. Sanvitto, S. Pigeon, A. Amo, D. Ballarini, M. De Giorgi, I. Carusotto, R. Hivet, F. Pisanello, V. G. Sala, P. S. S. Guimaraes, R. Houdré, E. Giacobino, C. Ciuti, A. Bramati, and G. Gigli, Nat. Photonics **5**, 610 (2011).

[27] F. Manni, T. C. H. Liew, K. G. Lagoudakis, C. Ouellet-Plamondon, R. André, V. Savona, and B. Deveaud, Phys. Rev. B, **88**, 201303(R) (2013).

[28] F. Manni, Y. Léger, Y. G. Rubo, R. André, and B. Deveaud, Nat. Commun. **4**, 2590 (2013).

[29] V. G. Sala, D. D. Solnyshkov, I. Carusotto, T. Jacqmin, A. Lemaître, H. Terças, A. Nalitov, M. Abbarchi, E. Galopin, I. Sagnes, J. Bloch, G. Malpuech,and A. Amo, arXiv: 1406.4816.

[30] Zh. Li, M. Zhang, G. Liang, X. Li, X. Chen, and Ch. Cheng, Opt. Express **21**, 15755 (2013).

[31] J. Sun, X. Wang, T. Xu, Zh. A. Kudyshev, A. N. Cartwright, and N. M. Litchinitser, Nano Lett. **14**, 2726 (2014).

[32] Y. Gorodetski, A. Niv, V. Kleiner, and E. Hasman, Phys. Rev. Lett. **101**, 043903 (2008); H. Kim, J. Park, S. W. Cho, S. Y. Lee, M. Kang, and B. Lee, Nano Lett. **10**, 529 (2010); P. Zilio, E. Mari, G. Parisi, F. Tamburini, and F. Romanato, Opt. Lett. **37**, 3234 (2012); Yu. Gorodetski, A. Drezet, C. Genet, and Th. W. Ebbesen, Phys. Rev. Lett. **110**, 203906 (2013).

[33] M. R. Matthews, B. P. Anderson, P. C. Haljan, D. S. Hall, C. E. Wieman, and E. A. Cornell, Phys. Rev. Lett. **83**, 2498 (1999).

[34] See Supplemental Material at http://link.aps.org/supplemental/10.1103/PhysRevLett.113.200404, for details of the experimental setup, condensate formation, imaging, and creation of higher-order orbital angular momentum states.

[35] M. Wouters, I. Carusotto, and C. Ciuti, Phys. Rev. B **77**, 115340 (2008).

[36] The errors in Fig. 4 are dominated by systematic effects. At low pump powers below the threshold for the condensation, the predominant source of errors (∼30%) is the ability to discriminate the low intensity condensate modes from the large thermal background. At higher pump powers, the errors are significantly reduced and stem from our ability to isolate each of the condensate modes, and to a lesser extent from the process of background subtraction (∼12%).

[37] M. Wouters and I. Carusotto, Phys. Rev. Lett. **99**, 140402 (2007).

[38] We choose the physical parameters close to those determined for our experimental sample, i.e., $m_{LP} = 10^{-4} m_e$, $g_c = 6 \times 10^{-3}\,\mathrm{meV}\,\mu\mathrm{m}^2$, $g_R = 2g_c$, $\gamma_c = 0.1\ \mathrm{ps}^{-1}$, $\gamma_r = 3.5\gamma_c$, and $R = 0.01\ \mu\mathrm{m}^2\,\mathrm{ps}^{-1}$. Here, m_e is the electron mass in vacuum.

[39] L. A. Smirnov, D. A. Smirnova, E. A. Ostrovskaya, and Yu. S. Kivshar, Phys. Rev. B **89**, 235310 (2014).